

ADVANCED INDUSTRIAL APPLICATION OF CFD FOR HELICOPTER DEVELOPMENT

Markus Dietz*, Dieter Schimke*, Martin Embacher**

*Eurocopter Deutschland GmbH
Willy-Messerschmitt-Straße
81663 München

**Institut für Aerodynamik und Gasdynamik
Universität Stuttgart
Pfaffenwaldring 21
70569 Stuttgart

Abstract

The present paper gives an overview on current activities at Eurocopter Germany related to advanced application of CFD for rotor and helicopter aeromechanics. The ongoing development of the aeromechanic tool environment is discussed and examples of advanced loosely coupled rotor and helicopter computations are provided. The examples address two key elements of advanced application of loose CFD/comprehensive code coupling: Firstly the extension of the coupling towards complete helicopter coupling and trim. The EC145 helicopter in steady forward flight was computed using complete helicopter coupling between FLOWer and Eurocopter's comprehensive code HOST. Trim convergence properties and computational effort are assessed and compared to isolated rotor studies. The benefits of complete helicopter coupling and trim for helicopter performance prediction are evaluated within an industrial context. The second issue is the extension of isolated rotor coupling towards more challenging cases. Loose coupling between FLOWer and CAMRAD II is applied to an isolated rotor in steady turn flight condition. Trim convergence is assessed and blade load results are compared to flight test data. Potential future benefit from CFD coupling for industrial design purposes is evaluated.

1. NOMENCLATURE

1.1. Trim Numbering

- The initial trim of the comprehensive code is denoted as 0th trim.
- The FLOWer calculation following the nth comprehensive code trim is denoted as nth FLOWer trim.

1.2. Acronyms

ADT	Alternating Digital Tree
ALE	Arbitrary Lagrangian Eulerian
CAMRAD II	Comprehensive Analytical Model of Rotorcraft Aerodynamics and Dynamics
CFD	Computational Fluid Dynamics
CHANCE	Complete Helicopter Advanced Computational Environment
DLR	Deutsches Zentrum für Luft- und Raumfahrt e.V.
ERF	European Rotorcraft Forum
GCL	Geometric Conservation Law

GUI	Graphical User Interface
HeliCATS	Helicopter Coupling and Trim Script
HOST	Helicopter Overall Simulation Tool
IAG	Institut für Aerodynamik und Gasdynamik, University of Stuttgart
KTAS	Knots True Air Speed
MUSIHC	Multidisziplinäre Simulation des Helicopters
SHANEL	Simulation of Helicopter Aerodynamics, Noise and Elasticity

2. INTRODUCTION

At last year's ERF Forum Eurocopter presented its activities concerning the realization of a loose coupling method between the CFD solver FLOWer (DLR) and the comprehensive helicopter code CAMRAD II. Loose coupling was applied to an isolated rotor in steady forward flight and promising results have been obtained for blade loads and rotor performance [1]. The trim procedure was restricted to the rotor.

Within the last year Eurocopter and its research partner IAG have continuously worked on the extension of the loose coupling framework between CFD and comprehensive helicopter codes. The aim of this work is twofold:

- The first objective is the extension of the loose coupling interface towards coupling and trim of the complete helicopter. From this measure we expect clear improvements with respect to the prediction of performance and loads due to the inherent potential of CFD to predict interactional aerodynamics. The necessity of this measure was already discussed in [1] and [2].
- The second objective of the work is to extend the boundary of loosely coupled isolated rotor computations towards more advanced flight cases. One major issue is to evaluate its potential for highly loaded rotors, e.g. rotors in turn flight condition. Here, industry is still lacking of a reliable prediction method for blade loads.

Complete helicopter coupling and trim is realized in a combined effort between Eurocopter and IAG. Eurocopter focuses on the extension of the coupling between FLOWer and CAMRAD II, whereas the IAG realizes the complete helicopter coupling and trim using FLOWer and HOST. The application of two different comprehensive codes is related to the individual strengths of the codes: The purpose of FLOWer/HOST coupling is mainly the improvement of helicopter performance prediction, whereas FLOWer/CAMRAD II coupling is predominantly used for blade loads prediction. A complementary paper related to the dynamics discipline evaluates the benefits of CFD coupling for vibratory loads prediction [3].

This paper presents two examples for complete helicopter trim with CFD coupling. The first test case uses CAMRAD II for trimming. Coupling with CFD is restricted to the main rotor. At the same time the CFD grid system includes only the main rotor. The second test case utilizes complete helicopter coupling: HOST trims the complete helicopter and coupling with CFD is performed on the main rotor, the fuselage and the tail rotor.

The second objective – the extension of the boundary of loose coupling towards more advanced cases – is covered by a coupled FLOWer/CAMRAD II computation of an isolated rotor in steady turn flight condition at a load factor of 1.53 and 50° bank angle. Blade load results are compared to flight test data.

The feasibility of applying loose coupling to advanced flight cases and complete helicopters is demonstrated by the examples in this paper. What is still missing is the integration into a generalized coupling framework. The paper provides insight into the ongoing tool development efforts, finally aiming towards the realization of a common modular coupling environment to be used in the industrial design process.

3. COMPUTATIONAL METHODS

3.1. HOST

Eurocopter's in-house rotorcraft comprehensive code HOST [4] is mainly used for flight mechanics purposes and enables the study of single helicopter components like isolated rotors as well as complete configurations with related substructures.

HOST trims the rotor based on a lifting-line method with 2D airfoil tables. Airframe component aerodynamics is provided by polars, either obtained from wind tunnel measurement or computed from CFD. For stand alone simulations various interference models are available in order to account for the interference effects between the individual components of the helicopter.

HOST includes an elastic blade model which considers the blade as a quasi one-dimensional Euler-Bernoulli beam. It allows for deflections in flap and lag direction and elastic torsion along the blade axis. In addition to the assumption of a linear material law, tension elongation and shear deformation are neglected. However, possible offsets between the local cross-sectional centre of gravity, tension centre and shear centre are accounted for, thus coupling forces and moments.

The blade model is based on a geometrically nonlinear formulation, connecting rigid segments through virtual joints. At each joint, elastic rotations are permitted about the lag, flap and torsion axes. Since the use of these rotations as degrees of freedom would yield a rather large system of equations, the number of equations is reduced by a modal Rayleigh-Ritz approach. A limited set of mode shapes together with their weighting factors are used to yield a deformation description. Therefore, any degree of freedom can be expressed as

$$h(r, \psi) = \sum_{i=1}^n q_i(\psi) \cdot \hat{h}_i(r)$$

where n is the number of modes, q_i the generalized coordinate of mode i (a function of the azimuth angle ψ), and \hat{h}_i is the mode shape (a function of the radial position r). It is obtained by an eigenvalue analysis of the beam in vacuum.

3.2. CAMRAD II

The commercial aeroelastic analysis code for helicopters and rotorcraft CAMRAD II incorporates a combination of state-of-the-art technologies like multibody dynamics, nonlinear finite elements, structural dynamics and rotorcraft aerodynamics [5].

The aerodynamic modelling of rotor systems in CAMRAD II is based on lifting line theory assuming that the rotor blade has a high aspect ratio, or more generally that spanwise variations of the aerodynamic environment are small. This assumption allows the problem to be split into separate blade wing and rotor wake models, which are solved individually

and combined. Two-dimensional, steady airfoil data are extracted from airfoil tables for solving the wing problem. Code-internally the coefficients are corrected for Mach and Reynolds effects, yawed flow and unsteady behaviour (Dynamic Stall modelling). Regarding the wake problem the induced velocity distribution on the rotor disk is either derived by analytical downwash models or computed by prescribed or Free-Wake methods.

For all structural dynamic elements of CAMRAD II, the rigid body motions can be large due to multibody dynamics, and the kinematics of the interfaces and rigid body motion are always exact. For the finite beam elements [7], the elastic motion is represented in addition by the deflection, extension, and torsion of the beam axis. The beam element implemented in CAMRAD II offers three different geometric models ranging from exact kinematics of the beam elastic motion to retaining only second-order effects of elastic motion in the strain energy and kinetic energy, restricting the elastic motion to moderate deflection. The beam element features in addition two structural models. The first structural model is beam theory for anisotropic or composite materials, the second structural model is based on Euler-Bernoulli beam theory for isotropic materials with an elastic axis, the undistorted elastic axis straight within the component. For the numerical models used in this paper, the second option was applied.

3.3. FLOWer

The CFD solver FLOWer [8] was compiled by DLR in the framework of the MEGAFLOW project [9] and is available at Eurocopter through the cooperation with DLR in the framework in CHANCE [10] and SHANEL [11] projects.

FLOWer solves the three-dimensional, compressible and unsteady Reynolds-Averaged Navier-Stokes equations. The equations are formulated in a non-inertial rotating reference system with explicit contributions of centrifugal and Coriolis forces to the momentum and energy equations. Furthermore FLOWer includes the ALE-Formulation which facilitates the computation of deforming meshes by adding whirl-fluxes resulting from the cell face motion to the convective flux portion. The Geometric Conservation Law (GCL) evaluates the cell volumes of the deformable mesh consistent to the cell face velocities. This ensures the preservation of uniform flow on deformable grids.

The discretization of space and time is separated by the method of lines. FLOWer includes a cell-vertex and a cell-centred formulation. Convective fluxes are computed using the JST scheme [12] which uses 2nd order central differences with artificial dissipation for stabilization. The integration in pseudo time is carried out using a 5-stage hybrid Runge-Kutta method. In order to circumvent the time step limitation of the explicit scheme FLOWer makes use of the dual time stepping technique with a second order implicit time

integration operator in case of unsteady flow [13]. FLOWer features the Chimera-technique allowing for arbitrary relative motion of aerodynamic bodies [14]. Relative motion of grids can be arbitrarily defined via the input file by setting up the required kinematic chain of coordinate systems. Chimera connectivities are determined using hole cutting and interpolation. The ADT search method is applied in order to identify donor cells in curvilinear grids.

Within the past years additional helicopter specific features have been integrated into FLOWer mainly by IAG [15]. This includes interfaces for time-accurate and loose coupling, a multi-block blade grid deformation tool and rotor specific post-processing. All loosely coupled computations presented in this paper were performed using the FLOWer code on CFD side.

4. TOOLS DEVELOPMENT

4.1. FLOWer Evolution

In order to prepare FLOWer for the later integration into a generalized coupling framework and in order to establish coupling on multiple rotors and the complete helicopter, the FLOWer code has been extended based on the previous HELI version of the code.

Loose coupling may now be defined on an arbitrary number of rotors. Each rotor may be topologically and geometrically different. The FLOWer rotor and blade load output has been significantly improved, now allowing for output in all relevant coordinate systems, i.e. geodetic system, helicopter fixed system, rotor fixed system and blade fixed system. In contrast to previous FLOWer HELI versions, the helicopter fixed system is explicitly defined within the hierarchical chain of FLOWer motion definitions. The helicopter fixed system may move unsteadily with respect to the geodetic system, allowing for the definition of arbitrary helicopter motions. This feature allows for the definition of e.g. a turn flight condition.

4.2. Coupling Environment

As mentioned earlier Eurocopter plans to integrate all developments related to helicopter aeromechanic simulation into a common, generalized coupling framework. The final goal is the provision of a generalized framework for the coupled flight mechanic, aerodynamic and structural dynamic analysis of helicopters. The HOST code is currently being reworked in order to establish general replacement of internal modules (e.g. aerodynamic or dynamic blade modelling) by external information.

As a preparation of a generalized coupling framework Eurocopter has integrated the loose coupling approach (see References [16] to [20] for details on loose coupling) between FLOWer and HOST and FLOWer and CAMRAD II into the common script

interface HeliCATS. The Python based script performs the sequential calls of FLOWer and the comprehensive codes as well as all intermediate data preparation tasks. In order to ease the setup of the coupled computation a Graphical User Interface has been set up. The graphical front end is shown in Figure 1. Besides the simplified preparation of the coupled run the GUI allows for online visualization of the trim convergence, adaptation of parameters during runtime (e.g. the number of time steps of the CFD runs) and automatic convergence detection. The script is already operational for a complete helicopter trim on comprehensive code side and isolated rotor CFD coupling for both FLOWer/HOST and FLOWer/ CAMRAD II couplings.

The integration of complete helicopter coupling procedure into the HeliCATS tool is currently ongoing. The coupled FLOWer/HOST complete helicopter analysis presented in this paper has still been performed using a manual data exchange between the codes for rapid prototyping purposes. More detailed information on the complete helicopter coupling procedure will be provided in section 6.1.

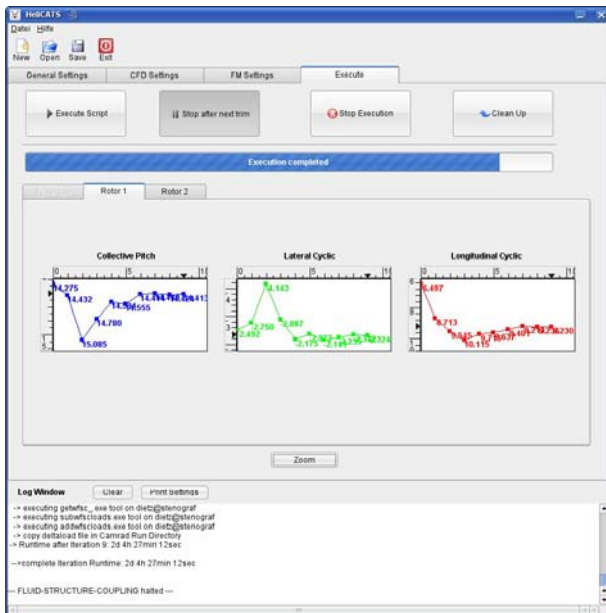


Figure 1: HeliCATS GUI

5. COMPLETE HELICOPTER TRIM

As a first step towards the trimmed surface-based modeling of the complete helicopter Eurocopter has extended its loose coupling environment towards a complete helicopter trim on comprehensive code side. Coupling with CFD is performed on the main rotor only, and the CFD grid system is restricted to the isolated rotor at the same time. Consequently, the aerodynamics of airframe and tail rotor is modeled purely by polars whereas the main rotor aerodynamics is replaced by CFD in the course of the loose coupling procedure.

The generic test case presented in the following applies loose rotor coupling between CAMRAD II and FLOWer. A complete helicopter trim is performed for the EC145 helicopter which is equipped with the hingeless rotor that was used for the investigations in [1]. The purpose of this study is the assessment of complete helicopter trimming with respect to robustness and computational effort, comparing with the previous isolated rotor trim procedure.

The main difference in the coupling procedure compared to an isolated rotor trim arises from the fact that the helicopter attitude is subject to change from one trim iteration to the following one. Consequently the main rotor shaft axis orientation relative to the flow has to be adapted on CFD side in order to account for the updated rotor inflow conditions. The number of free inputs on comprehensive code side increases from three to six: Main rotor collective, main rotor lateral and longitudinal cyclic, tail rotor pitch, helicopter pitch attitude and usually either helicopter roll attitude or helicopter sideslip. The latter is due to the fact that usually the helicopter is trimmed either for zero roll or for zero sideslip angle. Besides the tail rotor pitch setting all degrees of freedom need to be provided to the CFD solver in order to correctly consider the helicopter attitude and the main rotor control inputs.

Furthermore it should be noted that the trim target for the main rotor does not remain constant during the course of the coupling process. A complete helicopter trim requires vanishing forces and moments around the helicopter CG. As the helicopter attitude is set free, the rotor loads required to achieve this goal change from one trim cycle to the next.

The EC145 helicopter was trimmed at 135 KTAS and zero side slip. Automatic coupling using HeliCATS was performed. Figure 2 shows the trim convergence of this test case. The main rotor controls are plotted in the top Figure and the helicopter attitude as well as the pedal input is plotted in the bottom Figure. The Figure clearly illustrates that the convergence properties of the weak coupling scheme are not deteriorated by the inclusion of the additional degrees of freedom. If the trim Jacobian is well conditioned the scheme approaches equilibrium with the same speed, i.e. within the same number of coupling iterations.

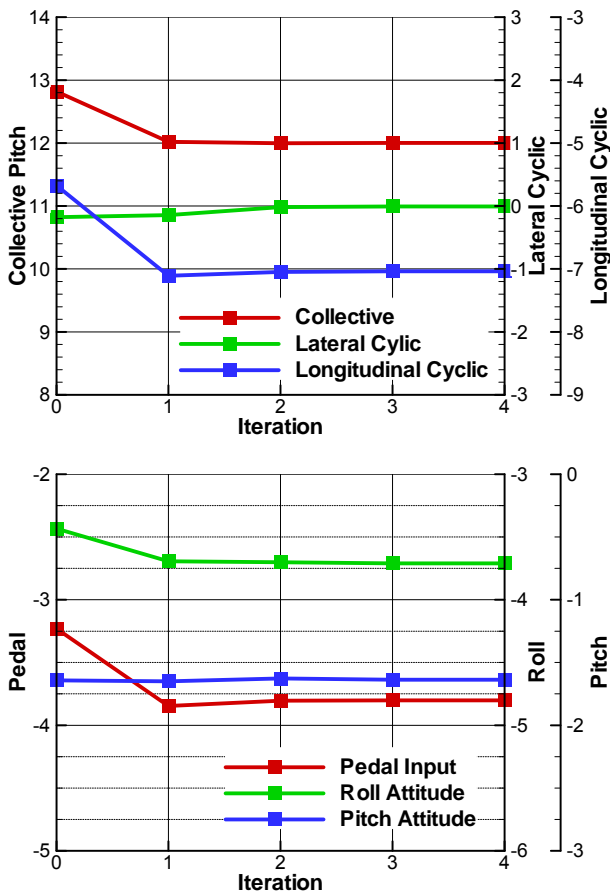


Figure 2: FLOWER/CAMRAD II complete helicopter trim convergence

The test case results indicate that complete helicopter trim with main rotor coupling does not feature any drawbacks with respect to robustness and computational effort. Compared to an isolated rotor trim it offers greater flexibility with respect to the trim law and is thus the more suitable approach for flight test recalculations.

6. COMPLETE HELICOPTER COUPLING

6.1. Coupling methodology

This section presents a complete helicopter coupling methodology between FLOWER and HOST. The major difference to the methodology presented in the previous section is the fact that coupling with CFD is not restricted to the rotor, but load exchange with the CFD solver is performed on main rotor, fuselage and tail rotor.

With respect to trimming, the statements of the previous section remain valid, i.e. the number of free control inputs increases from three to six: Three main rotor inputs, tail rotor collective, helicopter pitch attitude and either helicopter roll attitude or sideslip angle. The fundamental benefit of complete helicopter coupling is the fact that one makes direct use of the inherent capability of CFD to capture interference effects. All loads acting on the helicopter are

obtained from CFD and the final trim solution is purely based on CFD aerodynamics. Polar tables for the helicopter components are only required during the course of the loose coupling procedure in order to obtain the trim solution.

The coupling methodology is illustrated in Figure 3. Data exchange between CFD and comprehensive code is carried out in a loosely coupled manner, i.e. delta airloads are applied for all considered helicopter components on comprehensive code side.

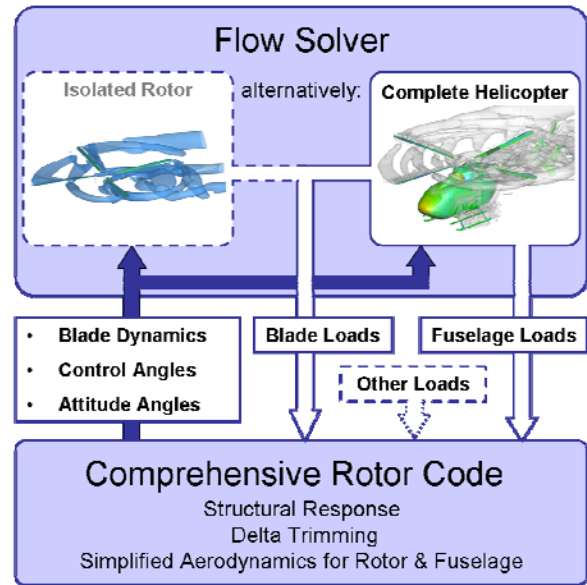


Figure 3: Complete helicopter coupling methodology

In this context it should be highlighted that the trim process in case of complete helicopter coupling is more challenging than the free flight trim process in case of pure isolated rotor coupling. In case of isolated rotor coupling the influence on the trim jacobian originating from the fuselage is purely polar based. In case of complete helicopter coupling CFD-corrected airloads are applied on the fuselage. If the aerodynamic characteristics in CFD differ too significantly from the polar based assumption trim convergence might be hampered. This case may arise e.g. if interference between rotor and horizontal stabilizer changes with the helicopter pitch attitude. Stability issues of the complete helicopter coupling procedure are discussed in [21].

6.2. Test case setup

The test case considered is the EC145 helicopter in level flight at 135 kts. The CFD mesh system is composed of 11 Chimera multi-block grid structures: the fuselage mesh, four main rotor blade meshes, two tail rotor blade meshes and four additional grid structures used for the skid landing gear. The fuselage mesh serves as a background mesh, i.e. it expands to the far field where characteristic boundary conditions are prescribed. The landing gear is not included in the fuselage mesh, but it is attached to the cabin bottom side using Chimera with over-

lapping walls. This strategy was chosen as it allows for an improved mesh quality and easy removal of the skid landing gear from the overall Chimera system. The overall number of grid cells is approximately 25 million.

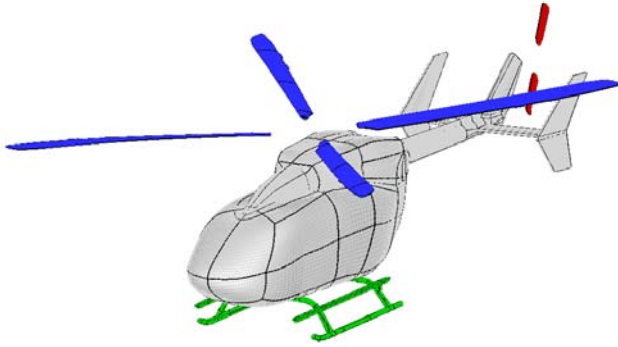


Figure 4: Surface mesh of complete helicopter configuration

Figure 4 shows the surface mesh of the CFD grid system. Note that the rotor head is not included in the CFD grid, predominantly in order to keep the amount of grid cells within an acceptable limit. The effect of the rotor head aerodynamics on the helicopter trim is considered by introducing an additional load corrective term on HOST side, see also Figure 3 (loads denoted as “Other Loads”). Here the rotor head polar is estimated from wind tunnel measurement data but it could also be included from CFD calculation.

During setup of the computation it was discovered that the landing skids lead to very high additional computational effort, mainly related to additional Chimera search and interpolation time. In order to reduce the computational effort, a landing skid interference study was performed. Trim iteration 0 was computed with and without skid landing gear. The interference effect on the helicopter is shown in Figure 5. It was decided to leave away the skid landing gear for all subsequent trim iterations, while introducing the skid loads and the interference loads as additional load correction terms for HOST. Skid loads and skid interference loads are assumed as constant during the course of coupling. This is a justified approximation as long as the effect of (small) helicopter attitude changes on the skid loads and skid interference loads are minor.

The actual coupling process was performed using manual data exchange between the codes. The integration of the data exchange procedure into the HeliCATS framework is currently ongoing.

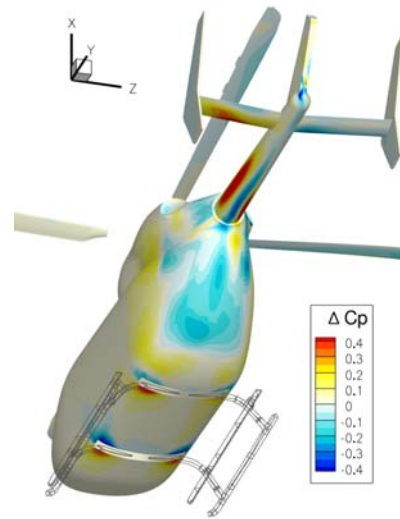


Figure 5: Landing gear interference effect on C_p distribution

Note that a special issue is the changing helicopter attitude during re-trim, resulting in varying inflow angles relative to the helicopter. This has to be accounted for in the CFD simulation. Principally different methods can be applied for this purpose: When using a dedicated background mesh and Chimera near-field meshes for all helicopter components, Chimera components can directly be rotated within the background mesh while conserving the inflow direction relative to the background. This strategy was used for the complete helicopter trim computation with isolated rotor coupling presented in the previous section. For the present computation, we have used whirl fluxes for the reorientation of the flow. Effectively, the helicopter is unsteadily piloted from its previous attitude into its new attitude using a specified number of physical time steps for this transition process. This strategy has proven to work well and features docile restart characteristics of the flow solver. In the meantime this strategy has been integrated into HeliCATS and the transition computation is performed automatically.

6.3. Results

Figure 6 shows the complex 3D flow field of the complete helicopter configuration. The interference of the main rotor wake with the helicopter aft body, tail boom, empennage and tail rotor can be easily identified. The complexity of the flow field clearly underlines the benefit of CFD to directly capture the interference effects between the individual components of the helicopter.

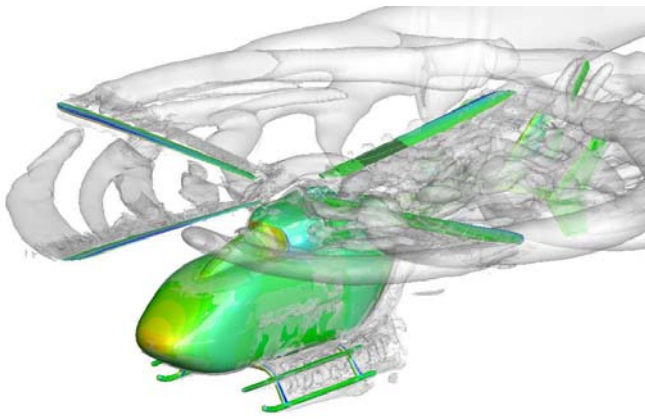


Figure 6: 3D flow field of complete helicopter configuration

Despite the considerable interference no convergence difficulties were observed during the loose coupling process. Note that the roll angle was prescribed according to the flight test value and the sideslip angle was set free.

Five trim iterations were necessary to reach convergence within the accuracy limit of the scheme. Development of the trim variables is shown in Figure 7 and Figure 8, plotting main rotor control angles, tail rotor thrust and fuselage attitude. The total number of iterations required to reach convergence is well in the range known from isolated rotor coupling and three-component wind tunnel trim. Initially a pronounced variation of trim variables takes place from trim cycle 0 to 1, which is caused by the substantial alteration of aerodynamic load modeling when adopting the correction terms from CFD. Any further trim changes, which then are required due to the differences between HOST prediction and actual CFD response, were observed to be smooth. A moderate overshoot in attitude and all rotor control angles except θ_S occurs, but no oscillations develop. An improvement over the HOST stand-alone prediction of the flight test is noted for all trim variables.

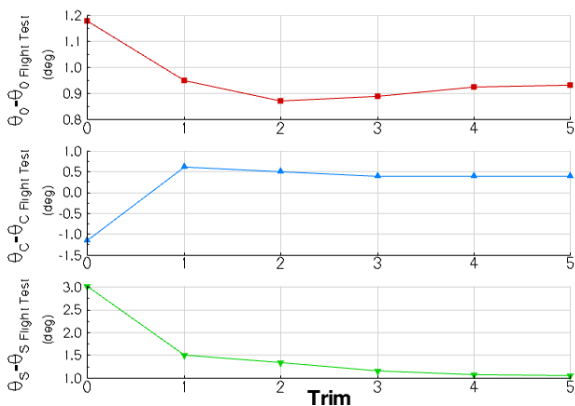


Figure 7: FLOWER/HOST complete helicopter trim convergence (main rotor inputs)

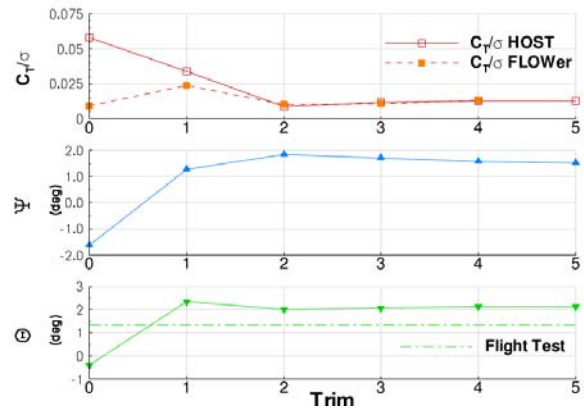


Figure 8: FLOWER/HOST complete helicopter trim convergence (helicopter attitude and tail rotor thrust)

Results have also been evaluated with respect to helicopter drag and performance.

For performance comparison the total engine power is available from flight test. It is measured via the engine torque at the drive shafts between the engines and the main gear box. Hence the measured power includes main gear box losses, tail rotor power and auxiliary device power. The main rotor power was separately measured via the shaft torque. The computational power consumption is extracted from the CFD result using the main rotor and tail rotor torques. The comparison of the power consumption must be considered as preliminary as the process for power extraction and evaluation is not yet fully consolidated for both sources.

Figure 9 shows a comparison of the computational result with the flight test value. The flight test performance is reproduced within only 4% deviation. This is a very good result, especially when considering that the coupled result is obtained without any additional tuning and taking into account that there are still deficiencies in the CFD numerical model. Note that comprehensive code simulations always need to be tuned using actual flight test performance data in order to facilitate accurate power reproduction. This is not the case for the coupled prediction method: The method claims to inherently reproduce power consumption, with accuracy increasing with rising level of detail of the CFD setup.

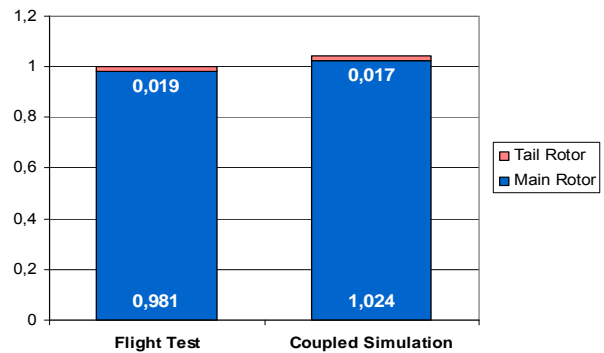


Figure 9: Helicopter power consumption

The computational CFD model still features some shortcomings. The elimination of these shortcomings

ings is likely to further increase the accuracy of power reproduction. The major simplifications for a better industrial applicability are:

- The computation is performed in fully turbulent manner. In [1] it was shown that consideration of transition will reduce the main rotor power consumption by roughly 3-4%.
- The rotor head is not included in the CFD model in order keep the computational effort within acceptable limits. However it has already been demonstrated that CFD is an efficient means to capture rotor head aerodynamics [22]. In the present study the effect of the rotor head on the helicopter trim has been taken into account by a load correction term based on wind tunnel data. The effect on rotor head wake interference is naturally not yet considered with the current CFD mesh system.
- The CFD model uses closed engine inlets and outlets. The EC145 features comparatively large inlets, causing a considerable amount of drag, if they are modelled as solid walls.
- Surface roughness details of the helicopter (antennas, door handles, etc.) are missing in the computational model. In the present case the drag overestimation caused by the engine inlets may counterbalance a drag underestimation caused by missing surface roughness.

The latter issue is illustrated in Figure 10 showing a drag breakdown on the individual helicopter components. The closed inlets/outlets contribute with about 15% to the overall fuselage drag. For our further investigations on this test case we plan to incorporate the engines by means of engine boundaries with prescribed mass flow at the engine inlets and outlets. In FLOWer engine boundary conditions are readily available and their application should not significantly increase the computational effort [23].

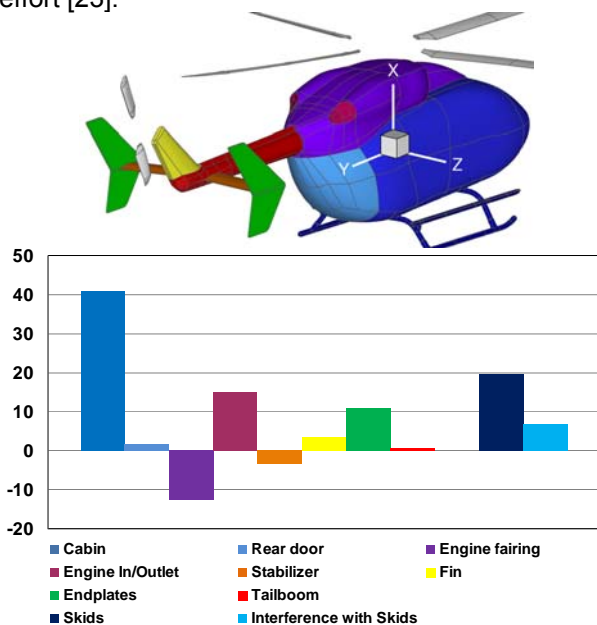


Figure 10: Fuselage drag breakdown (values in %)

7. ISOLATED ROTOR IN STEADY TURN FLIGHT CONDITION

7.1. Turn Flight Condition and Flight Test Data

The test case chosen for the coupled computation is identical to the one presented in last year's ERF paper [1], where we have validated the method using a steady level flight condition. The rotor is an experimental hingeless rotor featuring a Boelkow rotor hub and exchangeable blade tips. Flight test data are available from test campaigns on the BK117C1 helicopter. The experimental test bed is shown in Figure 11.



Figure 11: BK117C1 experimental test bed
(© Eurocopter Deutschland GmbH)

The turn flight condition is defined by flight test data. The relevant flight condition data are summarized in Table 1.

Helicopter weight	3370 kg
True Air Speed	109.4 KTAS
Far field pressure	80687 Pa
Far field temperature	5.0°C
Load factor	1.53g
Helicopter pitch attitude (nose up)	+1.0°
Helicopter roll attitude (roll right)	+50.9°
Helicopter descent rate	-1000ft/min

Table 1: Turn flight condition

As for the steady level flight computations presented in [1] we restrict the computational model to the isolated rotor on both comprehensive code (CAMRAD II) and CFD (FLOWer) side. Hence the isolated rotor is trimmed towards a given target. We trim the rotor for thrust and rotor pitch and roll moment. The rotor trim target is derived as follows: Pitch and roll moment were measured during flight test and can thus directly be used as trim targets. For the rotor thrust we use the simplified assumption

$$T = n_z \cdot mg$$

resulting in a C_T/σ of approximately 0.14.

Note that this is only a rough approximation as the additional lift created by the fuselage is not taken into account. Consequently the rotor thrust trim target is likely to be too high.

The main rotor collective and cyclic control angles are used as free control inputs. The helicopter attitude angles and the helicopter descent rate are directly prescribed from flight test and are not affected by the trim procedure.

It must be explicitly highlighted that this trim procedure is a first attempt and not yet fully consolidated. As already mentioned in the introduction, the purpose of performing loose coupling in steady turn flight is to evaluate the potential of CFD aerodynamics for blade loads prediction. Trimming the complete helicopter for power required, e.g. by setting free either pitch attitude or descent rate, would be a more appropriate trim law for this purpose. The decision for isolated rotor trim was made for its reduced complexity in terms of code-code coupling. The HeliCATS coupling architecture was readily available and validated.

Furthermore it should be mentioned that there is a certain level of uncertainty in the flight test data for helicopter attitude and descent rate. This issue results from the fact that, compared to a standard level flight case, sufficiently steady flight conditions are obtained only for a shorter time period. All of these aspects should be kept in mind when one evaluates the blade loads results.

Actually this is the first time loose coupling is applied to a turn flight condition. Predominantly, the test case should be considered as feasibility study for the principal applicability of loose coupling to highly loaded rotor cases, assessing aspects like test case setup, computational effort and coupling convergence with first priority and the actual quantitative blade loads results only with second priority.

7.2. Test case setup

On CFD side no changes were performed compared to the Chimera grid system used in [1]. Four Chimera near-body meshes for the blades are embedded into a Cartesian background mesh. The blade meshes use a multi-block topology with C-type topology in chordwise direction and O-type topology in spanwise direction. During the coupled computation the blade grids are deformed according to the current dynamic state of the blade using the multi-block grid deformation tool incorporated into FLOWer. The trailing edge tab configuration is identical to the one presented in [1].

The complete grid system consists of roughly 8 million grid cells. The $k\omega$ -Wilcox turbulence model was chosen for the closure of the RANS equations and an azimuthal resolution of 1° per time step was used.

The major difference compared to the steady forward flight case is given by the fact that the actual turn flight condition is prescribed in FLOWer using its rigid body motion capability. The flow is realized using grid motion, which guarantees a correct consideration of centrifugal and Coriolis forces and consequently a correct convection of the rotor wake and the tip vortex system. Note that it is not possible to map the flight state into a “wind tunnel”-like condition where a helicopter fixed in space experiences time-invariant inflow without streamline curvature.

The turn radius was estimated using the common flight mechanics relations, resulting in $R = 266\text{m}$. The yaw rate can be computed from the track speed of 109.4 kts and the descent rate of 1000ft/min, resulting in a value of $12^\circ/\text{s}$. The helicopter flight state is defined using the following kinematic chain of motions:

1. $\Omega = \text{const.}$ motion with yaw rate around FLOWer inertial system.
2. Radial translation of $r = 266\text{m}$ from turn center.
3. Vertical $v = \text{const.}$ motion with descent rate.
4. Pitch rotation.
5. Roll rotation.

The resulting relative system is the helicopter fixed system. The non-rotating rotor system is obtained by a translation from the helicopter CG into the hub center and a final pitch rotation around the rotor shaft installation angle. Figure 12 illustrates the position of the helicopter in the geodetic system (=FLOWer inertial system) for three subsequent rotor revolutions. The helicopter turn and descent motions can be easily identified. Note that the helicopter fuselage is only included for illustration purposes. The CFD computations were performed with the isolated rotor only.

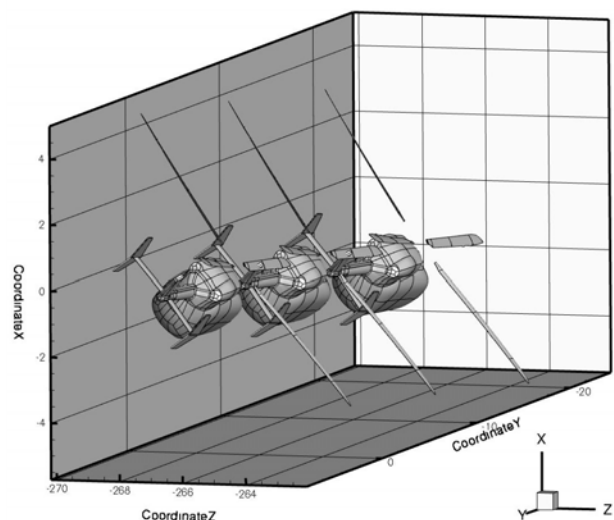


Figure 12: Helicopter position in FLOWer inertial system for three subsequent rotor revolutions

The CAMRAD II structural dynamic model of the rotor was not modified compared to the model used in [1]. An isolated rotor trim law was defined, prescribing the helicopter attitude angles, the helicopter track speed, descent rate and yaw rate. CAMRAD II determines related quantities like turn radius, helicopter angle of attack and rotor inflow angles. The values were checked for consistency with the corresponding FLOWER data.

7.3. Results

In Figure 13 unsteady rotor thrust and torque are shown for the complete weak coupling process. Each re-trim is marked off with respect to the preceding trim by the line type change from solid to dash and vice versa. It can be easily seen that both values approach a steady mean value. The prescribed thrust target is accurately met.

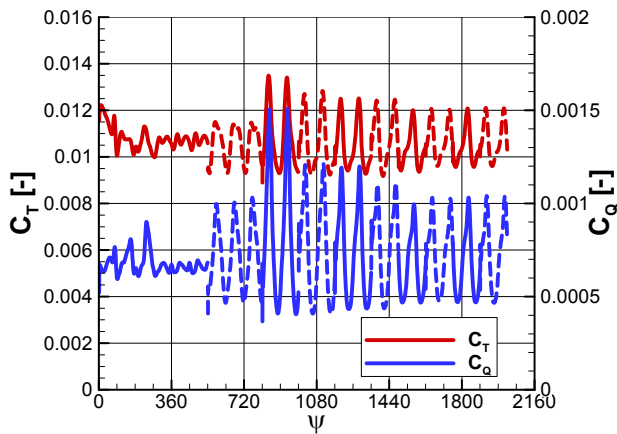


Figure 13: CFD thrust and torque versus the coupling iterations

The corresponding development of the free controls is given in Figure 14. When comparing with the corresponding plot in [1] one can see that more trim iterations are required in order to converge the control angles down to the usual convergence threshold of 0.01° . This does not come as a surprise as the aerodynamic rotor characteristics become more challenging with increasing rotor loading. This is also demonstrated by the fact that the control angles do not monotonously approach their final values. Instead the gradients change at trim iterations 2 and 3, respectively. This illustrates increased dependency of the elements of the trim jacobian from the actual control angle settings.

Nevertheless the trim convergence properties can be considered as robust. Figure 13 illustrates that, despite nine re-trim cycles, a converged solution can be obtained within less than six rotor revolutions.

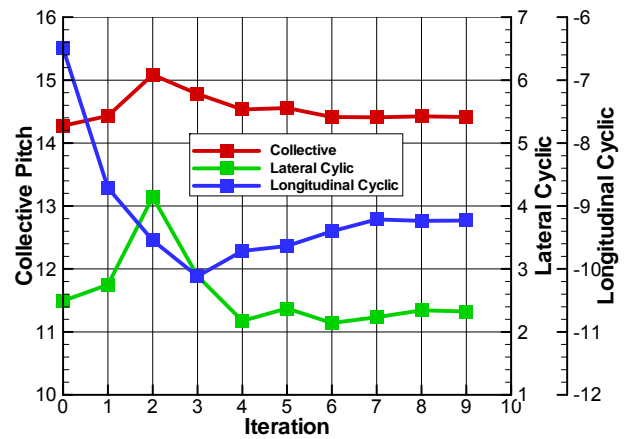


Figure 14: FLOWER/CAMRAD II turn flight trim convergence

Figure 15 shows the 3D flow field extracted from the converged CFD solution. The coordinate system used in the Figure corresponds to the one used in Figure 12. As a result of the coarse background mesh tip vortices are not conserved long enough to clearly identify the curvature in the vortex trajectories resulting from the turn flight condition. This is also due to the rather large turn radius with respect to the rotor diameter. Some indication of the turn rate and descent is provided by the tip vortex at the lower boundary of the Figure which is distorted towards port side.

A more important finding from the Figure is the fact that despite the high rotor thrust the blade tip vortices remain within the disk plane. This behaviour can be attributed to the helicopter pitch attitude and the rather high descent rate. Blade-vortex interaction phenomena can be clearly identified on several blades, e.g. at the outboard region of the retreating blade.

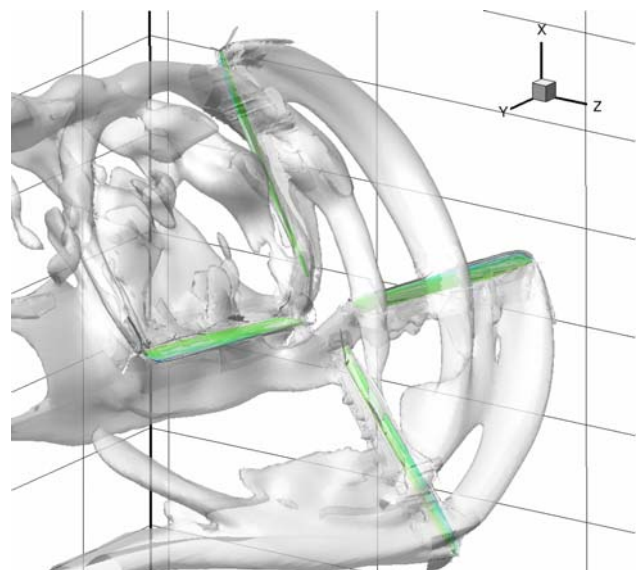


Figure 15: 3D flow field of rotor in turn flight

Figure 16 shows a detail of the previous Figure focussing on the outboard region of the retreating blade. The streamline patterns show reversed flow in the outboard region, possibly triggered by the interaction with the vortex. As a result of the coarse mesh and only 2nd order spatial accuracy of the numerical scheme the vortex has experienced a large dispersion and affects a wide spanwise region of the blade.

This may cause a general degradation of the retreating blade side prediction accuracy.

The possible thrust loss caused by the BVI phenomenon needs to be counterbalanced by an increased longitudinal cyclic pitch input and may also affect the rotor power consumption. A first rough evaluation reveals an overestimation of rotor power and a too high (too negative) longitudinal cyclic input compared to flight test. Quantitative results are not yet presented as evaluation is still ongoing.

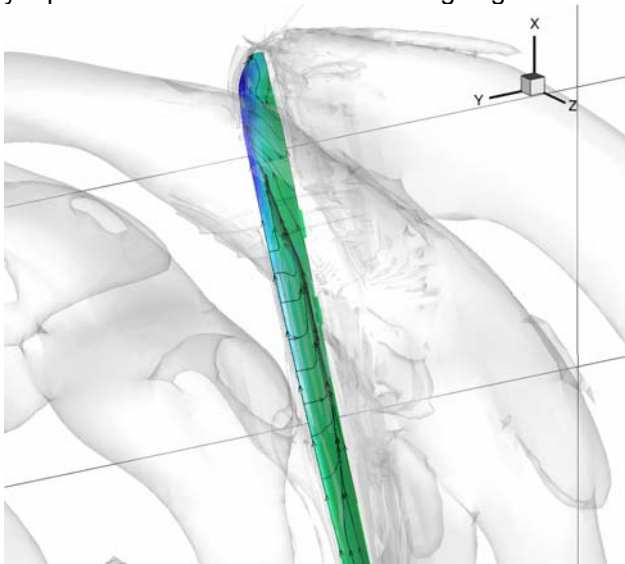


Figure 16: Retreating blade side flow and surface streamlines

Figures [15] to [18] show comparisons of the computed blade flap bending moments with the flight test measurements. The sensors are located at $r = 0.522\text{m}$, $r = 2.310\text{m}$, $r = 3.410\text{m}$ and $r = 4.510\text{m}$. The flight test data were recorded over 16 subsequent rotor revolutions. The scatter of the bunch of grey lines representing the recorded 16 revolutions is hence an indicator for the steadiness of the flight state. The black line represents the mean over all rotor revolutions using a low pass filter up to 10/rev. The Figures compare the azimuthal variation only, the mean values have been removed. The mean value is subject to the calibration of the strain gages (calibration in non-rotating state including blade weight) and hence different to the models. For this paper priority is given on the reproduction of Peak-to-Peak amplitude and frequency content which are more essential for assessing the maturity and the potential benefits of CFD plus coupling.

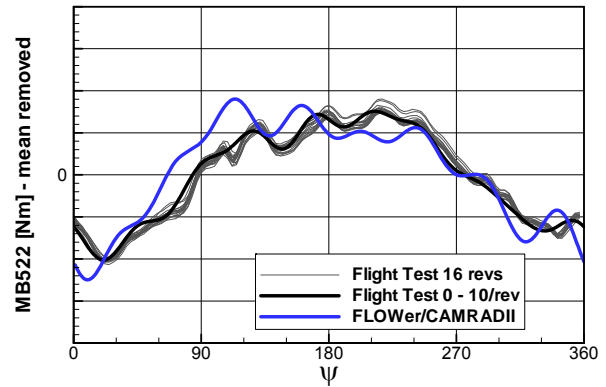


Figure 17: Flap moment at $r = 0.522\text{m}$

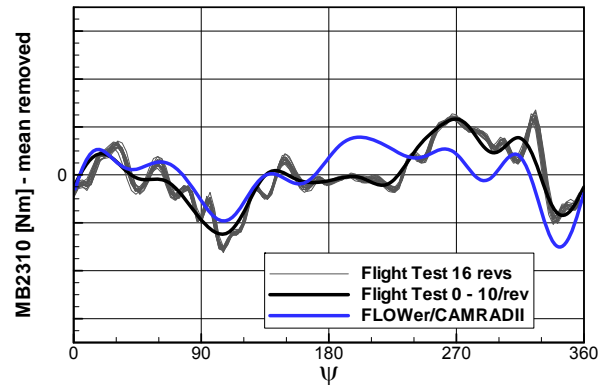


Figure 18: Flap moment at $r = 2.310\text{m}$

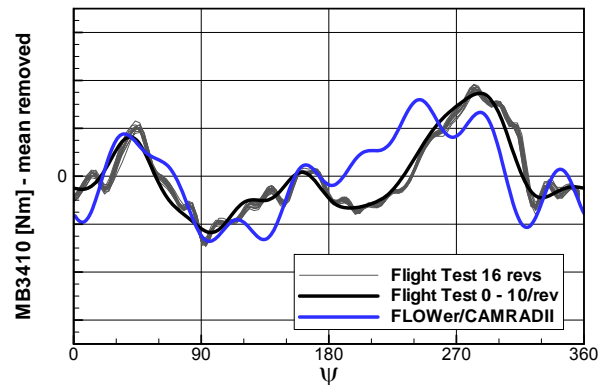


Figure 19: Flap moment at $r = 3.410\text{m}$

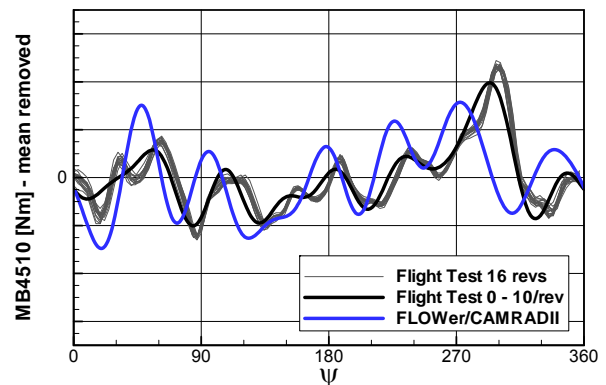


Figure 20: Flap moment at $r = 4.510\text{m}$

As a general statement one can note that the overall agreement is good for all sensors. Peak-to-peak values and frequency content (below 11/rev) are reproduced fairly well. By cross-comparing the Figures one notices that the coupled method is also able to capture the spanwise variation of the flap bending moment characteristics. Deviation to flight test is spotted in the range of $180^\circ < \psi < 240^\circ$, especially for the locations at $r = 2.310\text{m}$ and $r = 3.410\text{m}$, where the flap bending moment is overpredicted. The reason is not yet clear and further investigation is necessary.

Finally, Figure 21 shows a comparison of the lag bending moment at $r = 2.310\text{m}$. Again, peak-to-peak value and frequency content are well captured. However the phasing of the 4/rev contribution is not captured. This is possibly related to a missing drive train model which was not yet applied for this test case. The influence of the incorporation of a drive train model can be estimated from [3].

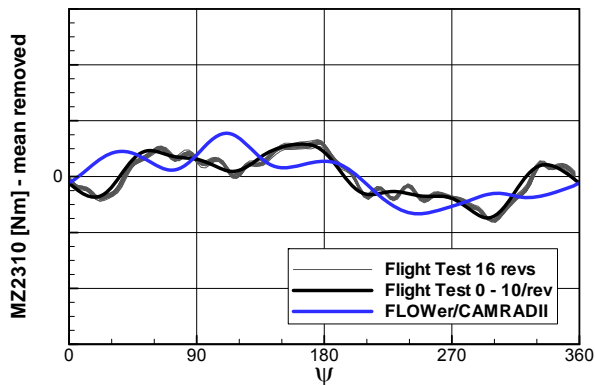


Figure 21: Lag moment at $r = 2.310\text{m}$

The first results presented in this section are encouraging and underline that loose coupling in steady turn for highly loaded rotors is feasible. As previously mentioned there are open issues to be further assessed: The isolated rotor trim procedure might be inaccurate and should be replaced by a complete helicopter trim and the accuracy of retreating blade side aeromechanics should be further assessed (grid refinement, turbulence modelling). Finally a thorough evaluation of blade torsion moment and pitch link load prediction capabilities needs to be performed. The coupled results need to be compared to stand-alone comprehensive code results in order to actually prove the benefits of CFD coupling.

8. CONCLUSION AND OUTLOOK

We have presented examples for advanced application of loose CFD/comprehensive code coupling in an industrial environment. The purpose of the activities is the improvement of prediction capabilities for helicopter performance and loads.

The studies on complete helicopter coupling and trim have shown the principal applicability of complete helicopter coupling and trim to tackle performance issues. Reasonable agreement is obtained for the performance prediction capability of the complete helicopter. This type of model can be applied in the industrial environment if a thorough selection is performed which components need to be fully included in the CFD trim process and which components can be incorporated by means of polars. In this context polars may either be generated by means of CFD pre-processing computations or may originate from wind tunnel tests.

The study on a highly loaded rotor in steady turn flight shows for the first time the wide range of applicability of the loose coupling approach. Challenging flight conditions like the one presented in the paper are required in the industrial helicopter design process for blade loads assessment.

The authors are confident to further improve Eurocopter's prediction accuracy by continued effort in this important area. Our final goal is the provision of an integrated coupling framework for the coupled aerodynamic, dynamic and flight mechanic simulation of the complete helicopter and the industrial evaluation of all intermediate steps towards this objective. Important steps towards this goal have already been realized and start to be used in the industrial design process.

ACKNOWLEDGEMENTS

The authors would like to thank the German ministry of Economy and Technology (BMW) for its funding in the framework of MUSIHC.

REFERENCES

- [1] Dietz, M., Dieterich, O.: "Towards Increased Industrial Application of Rotor Aeroelastic CFD", Proceedings of the 35th European Rotorcraft Forum, Hamburg, Germany, September 2009.
- [2] Dietz, M., Maucher, C., Schimke, D.: "Addressing today's Aeromechanic Questions by Industrial Answers", AHS Aeromechanics Specialists' Conference, San Francisco, CA, Jan 20-22, 2010.
- [3] Dieterich, O., Konstanzer, P., Dietz, M.: "Vibration Prediction in the Age of CFD", Proceedings of the 36th European Rotorcraft Forum, Paris, France, September 2010.
- [4] Benoit, B., Dequin, A-M., Kampa, K., Grünhagen, W. v., Basset, P-M., Gimonet, B.: "HOST: A General Helicopter Simulation Tool for Germany and France", American Helicopter Society.

- ety, 56th Annual Forum, Virginia Beach, Virginia, May 2000.
- [5] Johnson, W.: "Technology Drivers in the Development of CAMRAD II", AHS Aeromechanics Specialists' Conference, San Francisco, CA, 1994.
- [6] Johnson, W.: "A General Free Wake Geometry Calculation for Wings and Rotors", AHS 51st Annual Forum, Fort Worth, TX, 1995.
- [7] Johnson, W.: "Rotorcraft Dynamics Models for a Comprehensive Analysis", AHS 54th Annual Forum, Washington, DC, 1998.
- [8] Kroll, N., Eisfeld, B. and Bleecke, H.M., "The Navier-Stokes Code FLOWer", Volume 71 of Notes on Numerical Fluid Mechanics, pages 58-71. Vieweg, Braunschweig, 1999.
- [9] Kroll, N., Rossow, C.-C., Becker, K., Thiele, F.: "The MEGAFLOW Project", Aerospace Science and Technology, No. 4, 2000, pp. 223-237.
- [10] Costes, M., Pahlke, K., D'Alascio, A., Castellin, C., Altmikus, A.: "Overview of results obtained during the 6-year French-German CHANCE project", AHS 61st Annual Forum, Grapevine, TX, June 2005.
- [11] Costes, M., Raddatz, J., Borie, S., D'Alascio, A., Embacher, M.: "Advanced Rotorcraft Aeromechanics Studies in the French-German SHANEL Project", Proceedings of the 35th European Rotorcraft Forum, Hamburg, Germany, September 2009.
- [12] Jameson, A., Schmidt, W. and Turkel, E.: "Numerical Solutions of the Euler Equations by Finite Volume Methods Using Runge-Kutta Time-Stepping Schemes", AIAA-Paper 81-1259, 1981.
- [13] Jameson, A.: "Time Dependent Calculation Using Multigrid, With Applications to Unsteady Flows Past Airfoils and Wings", AIAA-Paper 91-1596, 1991.
- [14] Schwarz, Th.: "The Overlapping Grid Technique for the Time-Accurate Simulation of Rotorcraft Flows", Proceedings of the 31st European Rotorcraft Forum, Florence, Italy, September 2005.
- [15] Dietz, M.: „Simulation der Umströmung von Hubschrauberkonfigurationen unter Berücksichtigung von Strömungs-Struktur-Kopplung und Trimmung“, PhD Thesis, Verlag Dr. Hut, ISBN 978-3-89963-942-1, 2009.
- [16] Altmikus, A. Wagner, S., Beaumier, P., Servera, G.: "A Comparison: Weak versus Strong Modular Coupling for Trimmed Aeroelastic Rotor Simulations", American Helicopter Society 58th Annual Forum, June 2002.
- [17] Servera, G., Beaumier, P., Costes, M.: "A weak coupling method between the dynamics code HOST and the 3D unsteady Euler code WAVES", Proceedings of the 26th European Rotorcraft Forum, The Hague, The Netherlands, September 2000.
- [18] Pahlke, K., Van der Wall, B., "Calculation of Multibladed Rotors in High-Speed Forward Flight with weak Fluid-Structure-Coupling", Proceedings of the 27th European Rotorcraft Forum, Moscow, Russia, September 2001.
- [19] Potsdam, M., Yeo, H., Johnson, W.: "Rotor Airloads Prediction Using Loose Aerodynamic/Structural Coupling", AHS 60th Annual Forum, Baltimore, MD, June 2004.
- [20] Dietz, M., Altmikus, A., Krämer, E., Wagner, S.: „Weak Coupling for Active Advanced Rotors“, Proceedings of the 31st European Rotorcraft Forum, Florence, Italy, September 2005.
- [21] Embacher, M., Keßler, M., Dietz, M., Krämer, E.: „Coupled CFD Simulation of a Helicopter in Free-Flight Trim“, AHS 66th Annual Forum, Phoenix, AZ, May 11-13, 2010.
- [22] Le Chuiton, F., Kneisch, T., Schneider, S., Krämer, Ph.: "Industrial Validation of Numerical Aerodynamics about Rotor Heads: Towards a Design Optimization at Eurocopter", Proceedings of the 35th European Rotorcraft Forum, Hamburg, Germany, September 2009.
- [23] Le Chuiton, F.: „Quasi-steady Simulation of a Complete EC-145 Helicopter: Fuselage + Main / Tail Rotor Actuator Discs + Engines“, Proceedings of the 31st European Rotorcraft Forum, Florence, Italy, September 2005.